



Geopolymer Based Electrodes as New Class of Material for Electrochemical CO₂ Reduction

Jürgen Schuster,^[a] Neven Ukrainczyk,^{*[b]} Eddie Koenders,^[b] and Markus Stöckl^{*[a]}

To achieve a successful transition to a sustainable carbon and energy management, it is essential to both reduce CO₂ emissions and develop new technologies that utilize CO₂ as a starting substrate. In this study, we demonstrate for the first-time the functionalization of geopolymer binder (GP) with Sn for electrochemical CO₂ reduction (eCO₂RR) to formate. By substituting cement with Sn-GP, we have merged CO₂ utilisation and emission reduction. Using a simple mixing procedure, we were able to obtain a pourable mortar containing 5 vol. %

Sn-powder. After hardening, the Sn-GP electrodes were characterized for their mechanical and CO₂ electrolysis performance. In 10 h electrolyses, formate concentrations were as high as 22.7 ± 0.9 mmol L⁻¹ with a corresponding current efficiency of 14.0 ± 0.5% at a current density of 20 mA cm⁻². Our study demonstrates the successful design of GP-electrodes as a new class of hybrid materials that connect eCO₂RR and construction materials.

Introduction

The electrochemical conversion of CO₂ into carbon compounds (known as electrochemical CO₂ reduction reaction, eCO₂RR), presents various possibilities for use in chemical value chains and as a means for energy and carbon storage. It is a key technology for defossilization and can have a significant impact on the chemical industry. The choice of electrode materials is crucial for the success of electrochemical processes, with high activity, selectivity and stability being key requirements. However, for this technology to be widely implemented, the availability and cost-effectiveness of the electrode material must also be considered to ensure a favourable balance with the price of the electrochemical product.

A highly advanced eCO₂RR process with immense potential for industrial applications is the CO₂ reduction to formic acid or formate.^[1] The eCO₂RR to formic acid or formate has been extensively studied in literature^[2,3] and numerous publications demonstrate its superior performance, including high current densities (*j*) and current efficiencies (CE), durable electrode and process stabilities and high product concentrations.^[4–7] Thereby, formic acid/formate is a versatile molecule with promising applications in chemical industry. It can be used in organic

syntheses^[8,9], hydrogen storage,^[10–12] as a fuel for direct formic acid fuel cells^[13] and has been used as sustainable feedstock for microbially catalysed biosyntheses.^[14–16] Tin (Sn) and bismuth (Bi) represent the probable most applied electrocatalysts for the eCO₂RR to formic acid/formate due to their high selectivity towards formate, high abundance and the relative low costs compared to other selective electrocatalysts (e.g., indium).


In this study, we introduce a new class of electrode materials for the eCO₂RR by electrocatalytically functionalizing a geopolymer (GP) material with Sn. GP is an inorganic amorphous aluminosilicate polymer made from e.g. metakaolin and alkali silicate precursors and is currently being in research focus as an alternative building material in construction industry.^[17–23] GP can be used as a binder to substitute e.g., the established Portland cement (PC) in concrete and thereby inter alia drastically reduce CO₂ emissions of the CO₂ intensive construction sector,^[24] while still maintaining the material's strength, durability, performance and cost. To produce GP-based concrete, metakaolin is mixed with other functional additives and can be poured as a fresh mortar with similar properties to self-compacting concrete.^[25] The geopolymer mortar hardens quickly and forms a three-dimensional aluminosilicate network that is mechanically very stable and acid-resistant.


The GP-based concrete thus forms a low-cost basic structure that can incorporate other suitable functional materials, such as electrically conductive and/or electrocatalytically active materials, so that electrode materials can be produced from it. This offers a great opportunity for the large-scale production of inexpensive electrodes from functionalized/hybrid building materials.

In a previous study, we demonstrated that the addition of graphite to GP-mortar can lead to electrically conductive GP-electrodes.^[26] It was assumed that a graphite network was formed inside the GP, which allowed the application of the modified GP as electrode. We further demonstrated the successful application of the latter electrodes as inexpensive

[a] J. Schuster, Dr. M. Stöckl
Sustainable Electrochemistry
DECHEMA Research Institute
Theodor-Heuss-Allee 25, 60486 Frankfurt am Main (Germany)
E-mail: markus.stoeckl@dechema.de

[b] Dr. N. Ukrainczyk, Prof. Dr. E. Koenders
Institute of Construction and Building Materials
Technical University of Darmstadt
Franziska-Braun-Straße 3, 64287 Darmstadt (Germany)
E-mail: ukrainczyk@wib.tu-darmstadt.de

 Supporting information for this article is available on the WWW under <https://doi.org/10.1002/celec.202300122>

 © 2023 The Authors. ChemElectroChem published by Wiley-VCH GmbH. This is an open access article under the terms of the Creative Commons Attribution License, which permits use, distribution and reproduction in any medium, provided the original work is properly cited.

and robust anode material in microbial fuel cells (MFC).^[26] Based on these results, this study aims to demonstrate the application of functionalized GP-electrode materials as cathode material. Our previously reported design for conductive GP-electrodes was set as a benchmark and further functionalized by the addition of Sn-particles. Sn and graphite were added as electrochemically active catalyst and conductivity enhancing material to GP-mortar in a simple mixing routine to achieve new GP-electrode, for the cathodic synthesis of formate via the eCO₂RR.

Results and Discussion

Physical properties of geopolymer-based electrode material

As initial experiments, the characteristics of the Sn- and graphite-containing GP-mortar were examined to demonstrate the handling properties as raw and pourable material. These initial characterisations were performed to comprehensively characterize the new class of electrode material, which merges properties of construction and electrode materials. Workability test indicated good self-flowing characteristic, a self-flow table value of 20 cm (initial bottom radius of lifted conus is 15 cm), close to the upper limit of 23 cm set for Ordinary Portland Cement (OPC) by Okamura.^[27] Isothermal reaction calorimetry of the geopolymer hardening process showed a strong exothermic effect and very fast reaction kinetics for the hydrolysis/geopolymerisation, with the major part of the reaction taking place in the first days (Supporting Information S1, Figure S1). The addition of Sn additive resulted in intensification of the initial (dissolution) reaction kinetics, followed by retardation of the polymerization reaction kinetics within first day. The retardation agrees with findings on effects of Cu and ZnO, which we reported before.^[28] The reaction retardation effect is also observed in lower compressive strength results (Table 1). The initial metakaolin dissolution may be hindered by the formation of an amorphous Metal-hydroxide layer around the clay particles^[29] and poisoning the geopolymer gel nucleation.^[30–32] Compared to the unmodified GP (GP ref), both functionalized GP-mixtures show a decreased compressive strength after complete curing within 28 d. However, the effect of graphite (GP 10C; combined with water addition) had a more dominant role in reducing the compressive strength of plain GP (by factor 0.413), than the effect of Sn (combined, by factor of 0.326).

Table 1. Compressive strength results: effect of curing time, conductive additives, and electrochemical exposure. Results are reported as a mean of nine replicate measurements using one standard deviation to indicate measurement uncertainty.

Sample	Compressive strength [MPa]		
	7 d curing	28 d curing	After electrolysis
GP 10C 5Sn	11 ± 1	15 ± 2	35 ± 5
GP 10C	n.d. ^[a]	19 ± 1	n.d. ^[a]
GP ref	44 ± 2	46 ± 2	n.d. ^[a]

[a] n.d.: not determined.

More interestingly, compressive strength test of the Sn-modified GP electrodes (GP 10C 5Sn) after 34 h of electrochemical testing showed a significantly increased compressive strength by a factor of 2.35 (35 ± 5 MPa) compared to fresh GP 10C 5Sn electrodes.

As described in the results section on the electrochemical CO₂ reduction, a morphology change of the electrodes was observed during electrolysis. The precipitation of carbonates was observed on the outside of the electrodes and is assumed to also take place inside the porous Sn-GP electrodes. Furthermore, the distribution of Sn on the electrodes surface changed during electrolysis from particles to a homogenous surface coverage. Both findings might result from a morphology/structure change of the GP leading to the increased stability (compressive strength) and shall be part of future mechanistic studies on electrode aging. Since the porosity of electrodes can influence local current densities, potentials, and pH values as well as mass transport of substrates or products, the fresh electrode materials were compared regarding their porosities and pore size distributions. The main contribution on the porosity change was found to originate from the addition of the graphite compared to the Sn (Figure 1), which agrees with compressive strength results. The total intruded porosity increased from 32.29 (GP) to 47.25 (GP 10C) and 45.37 (GP 10C 5Sn). Moreover, similar trend is observed for an effect of shifting the pore size distribution curve towards coarser pores; being almost completely dominated by the addition of graphite (and water), while Sn addition had very low contribution. Addition of Sn resulted in lower total porosity, which is expected due to the inclusion of solid metal phase, which partly replaces the porous GP 10C matrix. Results of water intrusion porosity (measured only on GP 10C 5Sn samples) of 48.3 ± 0.5% are in good agreement with mercury intrusion pore (MIP) measurement results. Good agreement between water and mercury intrusion porosimetry was observed previously on geopolymers.^[33]

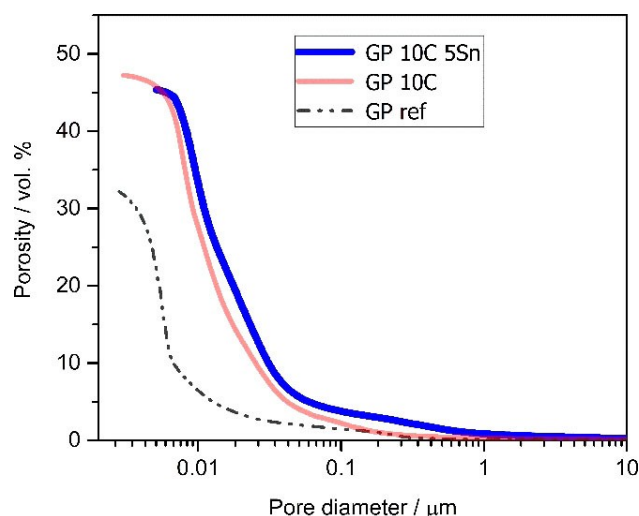


Figure 1. Pore size distribution measured with mercury intrusion pore of geopolymer based electrode materials: effect of graphite (GP 10C) and Sn (GP 10C 5Sn) addition on geopolymer (GP ref) microstructure.

As final physical property, the apparent air permeability was examined for the Sn-functionalized GP electrodes. The concept of air permeability is of importance in determining the transport characteristics of CO_2 through the electrode. Air permeability is a measure of how easily CO_2 can pass through the electrode material. This property is affected by pore water saturation level as well as open porosity and the pore geometrical structure (namely pore connectivity, tortuosity and constrictivity). Apparent air permeability of (GP 10C 5Sn9) sample resulted in a value of 0.58 ± 0.19 mD (equivalent to 5.7242×10^{-13} m²) showing an increased permeability compared to typical ranges for dense concretes (10^{-18} – 10^{-14}). To enhance air permeability, increasing the number of capillaries (specifically, pore sizes above 0.1 μm) is essential. This could be achieved by adjusting the grain size distribution and amounts of filler additives, such as Sn and carbon powders. These additives have been observed to increase pore sizes above 0.1 μm , as demonstrated in Figure 1.

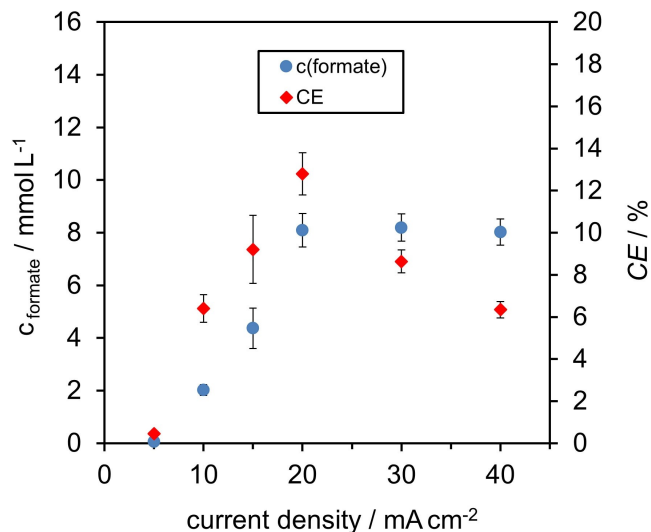


Figure 2. Average formate concentrations and average current efficiencies (with reference to formate conversions) determined from electrolyses carried out at different current densities of 5, 10, 15, 20, 30, and 40 mA cm^{-2} , respectively, with GP 10C 5Sn electrodes ($A_{\text{geometrical}} = 4.9 \text{ cm}^2$) in 0.5 M NaHCO_3 solutions. Standard deviations of 3 individual runs are shown in error bars. Sampling was done at the end of the electrolyses, after 4 h.

Electrochemical characterisations

The electrochemical characterization of the manufactured Sn-functionalized GP electrodes (GP 10C 5Sn) was performed in CO_2 -saturated NaHCO_3 solutions in galvanostatic operation mode. Initially, electrolyses were carried out at current densities (j) of 5, 10, 15, 20, 30 and 40 mA cm^{-2} , respectively, each with a duration of 4 h. As can be seen in Figure 2, a successful electrosynthesis of formate from the dissolved CO_2 could be achieved for all tested current densities, even though at a current density of 5 mA cm^{-2} almost no formate was detected (numerical values are given in Supporting Information S2, Table S2). As the current density increases, the obtained formate concentrations increase; at 20 mA cm^{-2} , the maximum CE of $12.8 \pm 1.0\%$ was observed at a formate concentration of $8.1 \pm 0.6 \text{ mmol L}^{-1}$ (Figure 2). For electrolyses carried out at higher current densities than 20 mA cm^{-2} , the CE for formate synthesis decreases to $8.6 \pm 0.6\%$ and $6.3 \pm 0.4\%$ for 30 and 40 mA cm^{-2} , respectively. This leads to the hypothesis that mass transport limitation (rather CO_2 /bicarbonate availability than product accumulation) become more dominant at current densities above 20 mA cm^{-2} . During all electrolyses, gas evolution was observed at the GP-electrodes surface. Due to the catalytic properties of Sn, it is assumed that the hydrogen evolution reaction (HER) is the main parasitic reaction, although the formation of carbon monoxide may also occur.^[2,34]

Since the eCO₂RR experiments with 20 mA cm^{-2} showed the best results in terms of produced formate and CE, 10 h electrolyses were conducted with the respective current density and the results are presented in Figure 3. The CO_2 conversion to formate during electrolysis with a current density of 20 mA cm^{-2} shows an increase in formate concentration over the whole period of 10 h up to a final value of $22.7 \pm 0.8 \text{ mmol L}^{-1}$ with a corresponding CE of $14.0 \pm 0.5\%$. Within the first 6 h both formate production rate and CE are continuously increased and in the further course up to 10 h, a relatively constant increase of approx. 2.3 mmol L^{-1} every hour was achieved (Figure 3A).

The increase in CE is higher at the beginning of the electrolysis within the first 4 h and reaches a rather constant value in the further time course (Figure 3B). The corresponding values for the cell voltage (U_c) are given in Supporting

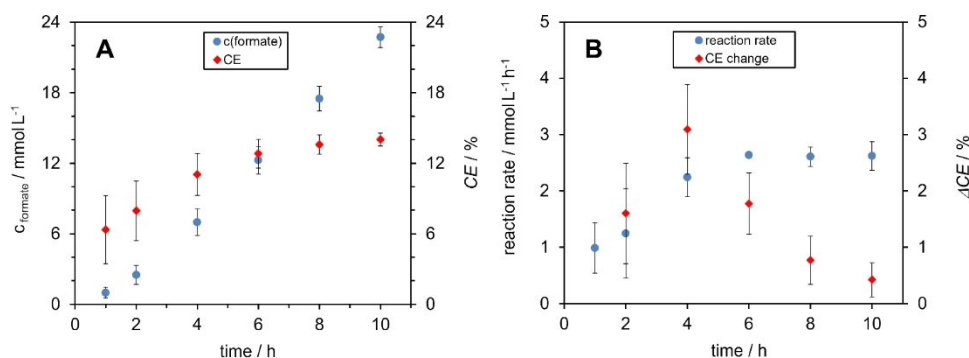


Figure 3. A) Average values of formate concentrations and average current efficiencies (CE) during electrolysis with GP 10C 5Sn electrodes in 0.5 M NaHCO_3 solutions at 20 mA cm^{-2} for 10 h. B) Corresponding average reaction rate for formate and changes in CE between the different sampling times during the 10 h electrolyses at 20 mA cm^{-2} . Standard deviations of 3 individual runs are shown in error bars.

Information S3 (Figure S3, Table S3). After about 6 h of electrolysis, the U_c starts to increase. Simultaneously, carbonate precipitates appear on the outside of the electrode, which become more with time. In addition to the carbonate precipitation, outer parts of the electrode also dissolve. After 10 h the outer side of the electrodes show strong signs of dissolution, whereas the inner side, i.e., the side facing the electrolyte, appears intact without signs of degradation. Photographs are shown in Supporting Information S4 (Figure S4).

These observations indicate that the performance of the electrode, which initially increases in the first 6 hours of electrolysis and then does not change significantly in the further course, is impaired by the carbonate precipitations. Various causes can be considered here. On the one hand, the precipitates can negatively influence the mass transport and slow down diffusion processes. On the other hand, electrochemically active centres in which the formate conversion takes place can be blocked. In both cases, the described processes can lead to an increase of the electrode potential in galvanostatic operation and thus to performance losses.

In all electrolysis experiments, small amounts of oxalate were found in the electrolyte solutions in addition to formate (Supporting Information S5, Table S5 and Supporting Information S6, Table S6). The highest concentration of $9.4 \pm 3.4 \mu\text{mol L}^{-1}$ was determined at the end of the 10 h electrolysis. In relation to the formate concentrations of $22.7 \pm 0.9 \text{ mmol L}^{-1}$ achieved during this experiment; this corresponds to a content of approx. 0.04% of the formate concentration. Since the focus of this study is on the feasibility of the electrochemical conversion of CO_2 to formate on functionalized geopolymer electrodes, the selectivity is not discussed in detail. The electrochemical conversion of CO_2 to oxalate is possible at high potentials,^[3] but this usually requires the use of non-aqueous/aprotic electrolytes.^[35] However, there are also approaches that make it possible to carry out the conversion with suitable catalysts at much lower overpotentials in aqueous media.^[36]

Influence of electrolysis on electrodes structure

As mentioned before, the appearance of the electrodes changes during the 10 h-electrolyses at 20 mA cm^{-2} and electrodes show signs of dissolution as the electrolysis time increases. However, this does not lead to a loss of their electrochemical performance during the observed electrolysis period since the highest CE is reached at the end of the experiment.

To compare the electrodes surfaces of unused electrodes and electrodes after the electrolysis, SEM/EDX images were taken. SEM images employing EDX for Sn mapping are presented in Figure 4. As can be seen, the unused electrode surface is characterized by a rather homogenous distribution of Sn particles on the electrode surface (Figure 4A). In contrast to this, images of the electrodes used in the electrolysis experiments show that the Sn particles dissolve/disappear from the electrode surface. Instead of distinct Sn-particles, elemental mapping images shows that Sn or SnO_x are finely distributed on

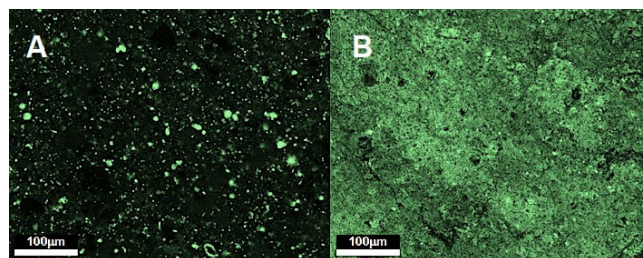


Figure 4. SEM/EDX element mapping of Sn (green) of an unused 5 vol.% Sn-geopolymer-electrode surface (left image) and of the surface facing the electrolyte of an electrode that was used in all experiments over a total period of approx. 34 h (right image).

the geopolymer electrode surface (Figure 4B and Supporting Information S7, Figure S7).

The change in Sn distribution on the electrode surface might result from several reasons. One possible hypothesis is the dissolution of Sn-particles due to high local pH-values at the electrochemically active Sn-particles.^[37] Due to the cathodic polarization of the GP-electrode, the dissolved Sn might be redeposited on the conductive electrode surface, which could explain the rather homogenous Sn-distribution on the electrodes surface. A second, eventually parallel effect might be the change of the geopolymer skeletal network. For a deeper understanding, XRD analysis of the applied Sn-powder (Supporting Information S8, Figure S8.1), an unused Sn-geopolymer electrode and an electrode after electrolysis (both in Supporting Information S8, Figure S8.2) were conducted. XRD analysis revealed, that the signal pattern typical for pure Sn-powder can also be found in the unused Sn-geopolymer electrodes. However, after electrolysis, a disappearance of the Sn peaks is found, which is assumed to be a result of the dissolution of the Sn-particles during the electrolysis. Furthermore, an increase of the amorphous hump centered around 30° 2Theta, which is typical for geopolymers,^[38,39] indicates a possible incorporation of Sn cations or Sn oxides into the geopolymer skeletal network,^[40] while formation of new diffraction peaks (Figure S8.2 and 8.3) indicate Sn oxidation into oxides (SnO , SnO_2) and hydroxides [$\text{Sn}_6\text{O}_4(\text{OH})_4$ and $\text{K}_2\text{Sn}(\text{OH})_6$].^[41,42]

Both findings, the electrode changes observed with SEM/EDX and XRD strongly indicate that a modification of the Sn-particles that takes place during electrolysis, which needs to be addressed in future studies. ICP-OES analyses of the Sn, Al, and Si contents of the electrolytes from working electrode chambers, of the experiments carried out at different current densities show that relatively small amounts of Sn enter the electrolytes. However, a trend can be seen that at high current densities the concentrations of the analysed elements increase (the results are presented in Supporting Information S9, Figure S9 and Table S9, respectively). Nevertheless, the results of the electrolyses demonstrate the successful operation and a stable formate synthesis with Sn-functionalized GP-electrodes, an aluminosilicate network that forms the framework of the electrode in which the added Sn and graphite are embedded.

Conclusion

In this study we demonstrate for the first-time the functionalization of a geopolymer with Sn for electrochemical formate synthesis from CO₂. Our approach allows to produce low-cost electrodes by simply mixing of widely available base materials. By selecting appropriate mixing ratios, electrodes can be designed specifically for different applications. This opens up numerous possibilities to tailor functionalized construction materials through modifications of the GP-electrodes to become structural parts of a large-scale infrastructure. However, while our results represent a proof of principle, there is still room for improvement in terms of higher current densities, lower cell voltages and increased CE efficiency. To achieve this, future studies should focus on optimal composition of GP-electrodes by variation/increase of Sn and graphite contents to find the ideal compromise between material (structural) stability and electrochemical performance. Furthermore, changes in surface morphology, electrode durability, and the possible integration of Sn into the geopolymer skeletal network should be investigated to gain a better understanding of the electrode aging during electrolysis.

The possibility of producing construction materials that emit significantly lower amounts of CO₂ during fabrication and enable further CO₂ reduction through electrochemical CO₂ electrolysis is a highly promising approach for new multifunctional construction materials. Our study demonstrates that CO₂ reduction to formic acid is feasible on Sn-geopolymer electrodes, and this low-cost electrode technology is suitable for electrochemical applications.

Experimental Section

Geopolymer-based electrode material preparation and physical characterization

Raw materials

Natural graphite (>99 wt.% purity) with a specific surface area of 10 m² g⁻¹ was used as conductive fine powder (90 vol.% of particles below 10 μm), exhibiting an electrical conductivity of 183 Sm⁻¹. Both precursors for geopolymer binder, metakaolin (characterisation details in^[43]) and potassium silicate solution (density 1.51 g cm⁻³, 45 wt.% solid content with SiO₂/K₂O ratio of 1.5) are commercial industrial products. Detailed characterization of used raw materials, except for the Sn additive, can be found in our previous publication.^[26] Polycarboxylate ether superplasticizer (PCE) was used to disperse powders. The Sn powder used (metallpulver24, Germany) contains spherical particles of pure Sn with a purity of ≥99.85% and a maximum particle size of 80 μm (sieve analysis: > 100 μm: 0.0%, > 71 μm: 0.2%, > 63 μm: 1.4%).

Preparation of electrode samples

Mix design of the electrode is based on optimized electrochemical performance, identified in our previous study.^[26] Mass ratios relative to metakaolin are 0.8, 0.63, 0.37 and 0.037 for silicate solution, water, graphite, and superplasticizer, respectively. This corresponds to 10 vol.% of graphite. To this reference mix, 5 vol.%

Sn powder was added, resulting in a 0.5668 mass ratio relative to metakaolin. To investigate the effect of Sn (and graphite) additives on geopolymerization reaction (kinetics) process and mechanical properties; three mixtures were prepared: geopolymer without additions (GP), with addition of graphite (GP 10C) and with Sn powder (GP 10C 5Sn).

Raw materials were mixed in a standard cement mortar mixer (E092-01 N, Mixmatic, Matest, Italy) designed for a total final volume of 768 mL to mold twelve (4 cm) cubic samples. First, graphite (155.7 g) was mixed with water (264.6 g) at 80 rpm for 90 s, to minimize absorption of silicate solution (added later). Separately, the PCE superplasticizer (15.6 g) was mixed with silicate solution (336.1 g). Then, the mixture of PCE with silicate solution was poured into the mixing bowl and stirred again at a mixing speed of 80 rpm. After 30 s, the stirring speed was increased to 285 rpm for 30 s. During a stirring pause of 30 s, the metakaolin powder (420.3 g) was added. After mixing at 80 rpm for 180 s, another stop for 30 s was used to manually scrape the mixer bowl (inside walls and bottom). The mixing continued at the same mixing speed for 180 s, followed by 285 rpm for 60 s. Finally, the Sn-powder (238.35 g) was added followed by mixing 80 rpm for 180 s and 285 rpm for 60 s. Workability properties are tested on a flow spread table according to DIN EN 1015-3 (for mortar), but without the 15-times lifting of the spread table, indicating good self-flowing value of 20 cm (initial bottom radius of lifted conus is 15 cm).

The fresh mortar was filled into plastic molds, using vibration (40 s at frequency of 40 rpm) to remove entrapped air bubbles. Two types of specimens were molded; 4 cm cubes for standard mechanical tests (9 samples), and cylinders of 5 cm in height and 4 cm in diameter for electrochemical and mechanical tests. Specimens were cured for 28 days at 20 °C. After the curing period cylindrical specimens were cut to 1 cm thick discs and dried at 50 °C for 2 weeks.

Physical electrode material characterisation

Mechanical stability

Compressive strength tests were carried out on standard cubic samples 4 cm at a loading rate of 2.4 kN s⁻¹ according to DIN EN 196-1 for cement mortars. Moreover, to investigate the change in mechanical properties after electrolysis experiments, 1 cm cubes were cut out from the discs (before and after exposure to electrochemical tests). Results are reported as a mean of nine replicate measurements using one standard deviation to indicate measurement uncertainty. The comparison of results between small and standard cubes showed no significant deviations (within the measurement deviation of the small cubes).

Pore size distribution

Mercury intrusion pore (MIP) measurements were performed using a Pascal 140 and 440 mercury intrusion porosimeter device (Thermo Fisher, Waltham, MA, USA), on dried samples (in oven at 60 °C until reaching a constant mass) taken from 28 d cured specimens. The pore diameter was calculated using Washburn's equation and parameters for mercury contact angle of 130°, density of 13.53 g cm⁻³ and surface tension of 0.485 N m⁻¹.

Water absorption

Measurements were applied on the dried 4 cm cubic specimens, by gradually immersing them in water under vacuum (10 Pa) for 24 h.

The dry mass, the water saturated mass and the sample volume (Archimedes method) were measured on at least three replicates (measurement uncertainty reported as mean \pm one standard deviation).

Air permeability

Air permeability was measured on dried disk (GP 10C 5Sn) samples using a Hassler cell permeameter machine. Result of apparent air permeability (in mD, mili darcy) is reported as a mean of three replicate measurements using one standard deviation to indicate measurement uncertainty. The apparent permeability was calculated using Darcy's equation on five subsequent measurements at different pressure gradients for each replicate, following procedure from Filomena et al.^[44]

Calorimetry

Isothermal reaction calorimetry was performed using a MC CAL device (from C3 Prozess- und Analysetechnik, Haar, Germany). For this, the total amount of material tested (24.7 g GP vs. 34.1 g GP 10C 5Sn) was corresponding to 10 g of the metakaolin powder.

Electrochemical characterisation and eCO2RR

Chemicals and reagents

All used reagents were of analytical grade: sodium bicarbonate p.A. (Merck); sodium formate EMSURE, p.A. (Supelco); dipotassium oxalate monohydrate, p.A. (VWR International); sulfuric acid 95–97% (Supelco); nitric acid Supra 69% (Roth); potassium, tin, aluminium and silicon single-element ICP-standard-solutions RotiStar 1000 mg L⁻¹ (Roth); CO₂ gas (5.0, Air Liquide). Deionized water (18.2 M Ω) was used to prepare all solutions and electrolytes.

Laboratory electrochemical H-cell and experimental setup

The sliced electrode discs (3.9 cm in diameter, ca. 1 cm thick) were examined in a H-cell setup, which can be used in anaerobic applications as described before.^[26,45] Briefly, the H-cell setup consisted of two modified 100 mL glass bottles, which were connected via flanges. In between the glass bottles, a circular proton-exchange membrane (Nafion 117, 4 cm in diameter, Sigma-Aldrich, St. Louis, USA) was inserted to separate the working electrode (WE) and counter electrode (CE) chambers. The WE were attached to the WE chamber with a clamping system via a second flange. A graphite foil (0.13 mm thick, RCT, Germany) was inserted between the flange of the WE chamber and the WE to establish an electrical contact. The inner diameters of the WE were 2.5 cm (geometrical $A_{WE}=4.9$ cm²). The CE chamber contained a DSA electrode (geometrical surface = 20 cm²). More detailed information and an image of a completely mounted H-cell are provided in Supporting Information S10.

Electrode imaging

Scanning electron microscopy (SEM) studies were carried out to investigate the composition of the geopolymer electrodes and the distribution of the Sn particles incorporated into the geopolymer. A Hitachi SU5000 (Hitachi, Chiyoda, Japan) equipped with a field emission electron gun source FE-SEM instrument fitted with a SE + BSE detector and EDX detector (Octane Elite Super, EDAX, Mahwah, USA) was used to image the electrodes. Prior to imaging, the air-

dried electrodes were dried in a vacuum chamber at 20 mbar for 30 min and then fixed with graphite tape to a sample stub. The sample stubs were placed directly into the SEM vacuum compartment and examined at an accelerating voltage of 20 kV. X-ray diffraction measurements were carried out with a Bruker D8 ADVANCE A25 (Bruker, Billerica, USA) equipped with a Cu X-ray tube to observe the phase and crystallinity changes before and after CO₂ electrolysis.

Liquid sample analysis

High performance liquid chromatography (HPLC) was used to determine formate and oxalate concentrations of the electrolyte samples taken during the CO₂ electrolysis experiments. A Shimadzu Prominence Modular HPLC with photodiode array detector SPD-M20A was used (Shimadzu, Kyōto, Japan), with a REZEX-ROA column (Phenomenex, California, USA) with 0.005 M sulphuric acid as eluent. A description of the method used can be found in the Supporting Information S11. To evaluate the stability of the electrodes, inductively coupled plasma with optical emission spectroscopy (ICP-OES) measurements were carried out. The electrolytes were tested for the elements potassium, tin, aluminium, and silicon. The ICP-OES used was an Agilent 5800 ICP-OES instrument. A description of the method used can be found in the Supporting Information S12 and Table S12.

Experimental electrolysis procedure

The electrolysis experiments were carried out at room temperature with a HMC 8043 power supply unit (Rohde & Schwarz, München, Germany) in two-electrode-setup, with 0.5 M NaHCO₃ solutions as electrolyte. The filling volume of the cathode and anode chambers was 120 mL each. and the chambers were stirred. In each case, 20 min prior to the start of an experiment, the catholyte was gassed with 60 mL min⁻¹ CO₂ to ensure CO₂ saturated electrolyte. The 0.5 M NaHCO₃ electrolytes used ensure good electrolytic conductivity, and with the addition of CO₂, a carbonic acid-bicarbonate buffer system is obtained, ensuring a constant concentration of bicarbonate during electrolysis, which is considered as reactive species in the reduction of CO₂ on metal and metal oxide electrodes.^[46,47] To test the suitability of the electrodes for CO₂ reduction all electrolysis experiments were carried out in triplicate.

Calculations

The current efficiency (CE) of electrochemically produced formate was calculated by the ratio between the measured amount of formate from the respective electrolysis and the theoretically possible amount of formate:

$$CE_{\text{formate}} = \frac{m(\text{formate})_{\text{experimental}}}{m(\text{formate})_{\text{theoretical}}} \times 100\% \quad (1)$$

Thereby, the theoretically possible amount of formate was calculated according to Faraday's law:

$$m(\text{formate}) = \frac{M \times I \times t}{z \times F} \quad (2)$$

With M as the molecular weight of formate (45.03 g mol⁻¹), I as the electrolysis current [A], t as the time [s], z as the number of electrons (2 e⁻), and F as the Faraday constant (96485 C mol⁻¹).

Author Contributions

Jürgen Schuster: Conceptualization (equal); Investigation (equal); Writing – Original Draft Preparation (lead). **Neven Ukrainczyk:** Conceptualization (equal); Investigation (equal); Writing – Original Draft Preparation. **Eddie Koenders:** Resources (equal). **Markus Stöckl:** Conceptualization (equal); Supervision (lead); Resources (equal); Writing – Review & Editing (lead)

Acknowledgements

The authors gratefully acknowledge the financial support by the German Federal Ministry of Economic Affairs and Climate Action (Grant nr: 21866N-1) and the project “PV-WALL” PZS-2019-02-1555 in Research Cooperability Program of the Croatian Science Foundation funded by the European Union. Special thanks to Dr. Jens Hornung (Applied Sedimentary Geology at TU Darmstadt) for providing air permeability measurements. Open Access funding enabled and organized by Projekt DEAL.

Conflict of Interests

The authors declare no conflict of interest.

Data Availability Statement

The data that support the findings of this study are available from the corresponding author upon reasonable request.

Keywords: electrochemical CO₂ reduction • formate • geopolymer electrode • Sn-functionalization • new electrode material

- [1] M. Stöckl, N. J. Claessens, S. N. Lindner, E. Klemm, D. Holtmann, *Curr. Opin. Biotechnol.* **2022**, *74*, 154–163.
- [2] Y. Hori, H. Wakebe, T. Tsukamoto, O. Koga, *Electrochim. Acta* **1994**, *39*, 1833–1839.
- [3] Y. Hori, *Mod. Aspects Electrochem.* **2008**, *42*, 89–189.
- [4] H. Yang, J. J. Kaczur, S. D. Sajjad, R. I. Masel, *J. CO₂ Util.* **2017**, *20*, 208–217.
- [5] R. B. Kutz, Q. Chen, H. Yang, S. D. Sajjad, Z. Liu, I. R. Masel, *Energy Technol.* **2017**, *5*, 929–936.
- [6] D. Kopljar, A. Inan, P. Vindayer, N. Wagner, E. Klemm, *J. Appl. Electrochem.* **2014**, *44*, 1107–1116.
- [7] A. Löwe, M. Schmidt, F. Bienen, D. Kopljar, N. Wagner, E. Klemm, *ACS Sustainable Chem. Eng.* **2021**, *9*, 4213–4223.
- [8] P. Ganapati Reddy, G. D. Kishore Kumar, S. Baskaran, *Tetrahedron Lett.* **2000**, *41*, 9149–9151.
- [9] M. Shin, J. Seo, Y. Baek, T. Lee, M. Jang, C. Park, *Biomol. Eng.* **2020**, *10*, 7–10.
- [10] K. Tedsree, T. Li, S. Jones, C. W. A. Chan, K. M. K. Yu, P. A. J. Bagot, E. A. Marquis, G. D. W. Smith, S. C. E. Tsang, *Nat. Nanotechnol.* **2011**, *6*, 302–307.
- [11] M. Grasmann, G. Laurency, *Energy Environ. Sci.* **2012**, *5*, 8171–8181.
- [12] M. Navlani-García, K. Mori, D. Salinas-Torres, Y. Kuwahara, H. Yamashita, *Front. Mater.* **2019**, *6*, 1–18.
- [13] R. Bhaskaran, B. G. Abraham, R. Chetty, *Wiley Interdiscip. Rev. Energy Environ.* **2022**, *11*, 1–31.
- [14] R. Hegner, K. Neubert, L. F. M. Rosa, F. Harnisch, *ChemElectroChem* **2019**, *6*, 3731–3735.
- [15] R. Hegner, K. Neubert, C. Kroner, D. Holtmann, F. Harnisch, *ChemSusChem* **2020**, *13*, 5295–5300.
- [16] M. Stöckl, S. Harms, I. Dinges, S. Dimitrova, D. Holtmann, *ChemSusChem* **2020**, *13*, 4086–4093.
- [17] B. B. Jindal, T. Alomayri, A. Hasan, C. R. Kaze, *Environ. Sci. Pollut. Res. Int.* **2022**, *30*, 25299–25324.
- [18] O. Vogt, N. Ukrainczyk, C. Ballschmiede, E. Koenders, *Materials (Basel)*. **2019**, *12*, 3485–3596.
- [19] O. Vogt, N. Ukrainczyk, E. Koenders, *Materials (Basel)*. **2021**, *14*, 5396.
- [20] S. Rocha Ferreira, N. Ukrainczyk, K. Defáveri do Carmo e Silva, L. Eduardo do Silva, E. Koenders, *Constr. Build. Mater.* **2021**, *288*, 123053.
- [21] Á. Palomo, S. Alonso, A. Fernandez-Jiménez, I. Sobrados, J. Sanz, *J. Am. Ceram. Soc.* **2008**, *87*, 1141–1145.
- [22] J. L. Provis, J. S. J. Van Deventer, *Geopolymers: Structures, Processing, Properties and Industrial Applications*, Woodhead Publishing Limited, New Delhi, **2009**.
- [23] J. Davidovits, *Geopolymer Chemistry and Applications*, Institute Geopolymère, San Quintin, **2008**.
- [24] G. Habert, C. Ouellet-Plamondon, *RILEM Tech. Lett.* **2016**, *1*, 17–23.
- [25] M. Thakur, S. Bawa, *Mater. Today: Proc.* **2022**, *59*, 1683–1693.
- [26] S. Zhang, J. Schuster, H. Frühauf-Wyllie, S. Arat, S. Yadav, J. J. Schneider, M. Stöckl, N. Ukrainczyk, E. Koenders, *ACS Omega* **2021**, *6*, 28859–28870.
- [27] H. Okumura, K. Ozawa, *Concr. Libr. Japanese Soc. Civ. Eng.* **1995**, *25*, 107–120.
- [28] C. Grengg, G. Koraimann, N. Ukrainczyk, O. Rudic, S. Luschnig, G. J. G. Gluth, M. Radtke, M. Dietzel, F. Mittermayr, *Cem. Concr. Res.* **2021**, *149*, 106541.
- [29] N. Ukrainczyk, N. Vrbos, J. Sipusic, *Adv. Cem. Res.* **2012**, *24*, 249–262.
- [30] M. R. Anseau, J. P. Leung, N. Sahai, T. W. Swaddle, *Inorg. Chem.* **2005**, *44*, 8023–8032.
- [31] N. Garg, C. E. White, *J. Mater. Chem. A* **2017**, *5*, 11794–11804.
- [32] L. Wang, D. A. Geddes, B. Walkley, J. L. Provis, V. Mechtcherine, D. C. W. Tsang, *Cem. Concr. Res.* **2020**, *136*, 106194.
- [33] O. Vogt, N. Ukrainczyk, C. Ballschmiede, E. Koenders, *Materials*. **2019**, *12*, 3485.
- [34] X. Zhang, S. X. Guo, K. A. Gandionco, A. M. Bond, J. Zhang, *Mater. Today* **2020**, *7*, 100074.
- [35] M. König, S. H. Lin, J. Vaes, D. Pant, E. Klemm, *Faraday Discuss.* **2021**, *230*, 360–374.
- [36] A. R. Paris, A. B. Bocarsly, *ACS Catal.* **2019**, *9*, 2324–2333.
- [37] F. Bienen, A. Löwe, J. Hildebrand, S. Hertle, D. Schonvogel, D. Kopljar, N. Wagner, E. Klemm, K. A. Friedrich, *J. Energy Chem.* **2021**, *62*, 367–376.
- [38] N. Ukrainczyk, O. Vogt, *RILEM Tech. Lett.* **2020**, *5*, 163–173.
- [39] C. Grengg, G. Koraimann, N. Ukrainczyk, O. Rudic, S. Luschnig, G. J. G. Gluth, M. Radtke, M. Dietzel, F. Mittermayr, *Cem. Concr. Res.* **2021**, *149*, 106541.
- [40] K. Kanie, M. Sakaguchi, F. Muto, M. Horie, M. Nakaya, T. Yokoi, A. Muramatsu, *Sci. Technol. Adv. Mater.* **2018**, *19*, 545–553.
- [41] S. Khalameida, M. Samsonenko, J. Skubiszewska-Zięba, O. Zakutnevskyy, *Adsorpt. Sci. Technol.* **2017**, *35*, 853–865.
- [42] I. A. Courtney, J. R. Dahn, *J. Electrochem. Soc.* **1997**, *144*, 2045–2052.
- [43] K. Weise, N. Ukrainczyk, A. Duncan, E. Koenders, *Materials (Basel)*. **2022**, *15*, 367.
- [44] C. M. Filomena, J. Hornung, H. Stollhofen, *Solid Earth* **2014**, *5*, 1–11.
- [45] M. Stöckl, N. C. Teubner, D. Holtmann, K. M. Mangold, W. Sand, *ACS Appl. Mater. Interfaces* **2019**, *11*, 8961–8968.
- [46] N. Srekanth, K. L. Phani, *Chem. Commun.* **2014**, *50*, 11143–11146.
- [47] S. Lee, J. D. Ocon, Y. Il Son, J. Lee, *J. Phys. Chem. C* **2015**, *119*, 4884–4890.

Manuscript received: March 18, 2023

Revised manuscript received: April 25, 2023

Version of record online: July 14, 2023